near-infrared region of the spectrum, not within the wavelength range which we can currently probe (400–700 nm). It is interesting to note that the time scale associated with the restructuring of $CrL_5(CH-C_3H_7O)$ to $CrL_5(O-C_4H_8)$ (L = CNPh, CO) is approximately 4 times longer in the case of the phenyl isocyanide complex. This difference in kinetics could be accounted for by changes in the metal–solvent bond strengths as well as steric considerations in the isocyanide complex.

The transient absorption data for $Cr(CNPh)_6$ show that excitation results in efficient bond cleavage followed by rapid solvent coordination. These results are in agreement with the conclusion of optical studies of $Cr(CO)_6$. In both molecules, evidence for the formation of a distribution of solvated complexes is observed. The time dependence of the absorption signal reveals the relaxation of silane coordinated complexes to the more stable oxygen coordinated intermediate.

Acknowledgment. This work is supported by the National Science Foundation. We thank Dr. Douglas Taube and Prof. Teddy Traylor for providing the sample of $Cr(CNPh)_6$.

Kinetics of the Methoxy Radical Decomposition Reaction: Theory and Experiment

M. Page,* M. C. Lin,*,†

Naval Research Laboratory, Washington, D.C. 20375-5000

Yisheng He, and T. K. Choudhury

Department of Chemistry, The Catholic University of America, Washington, D.C. 20064

The rate constant for the unimolecular decomposition of the methoxy radical, $CH_3O + M \rightarrow CH_2O + H + M$, is determined both theoretically and experimentally. In the theoretical calculations, potential energy surface information is obtained from ab initio multiconfiguration SCF and multireference configuration interaction calculations using basis sets of up to triple-ζ plus polarization quality. The zero point corrected forward and reverse barriers are calculated to be 25.6 and 8.0 kcal/mol, respectively. RRKM rate calculations are performed incorporating a quantum correction due to tunneling through an Eckart barrier fit to represent the MRCI/TZP energetics and the shape of the MC-SCF/DZP vibrationally adiabatic potential energy curve in the saddle point region. The calculated values compare closely with experimental data derived from kinetic modeling of CO formation rates measured in the thermal decomposition of methyl nitrite at 550–700 K in a static cell and at 1060–1620 K in shock waves.

Introduction

The methoxy radical is one of the most important and ubiquitous combustion intermediates; it is known to be present in almost all hydrocarbon and many other organic compound combustion reactions. The rapid breakdown of large alkyl groups at high temperatures ultimately gives rise to the smallest and most stable alkyl radical, CH_3, which can be readily oxidized to CH_3O by O_2, OH, and HO_2.[1]

The unimolecular decomposition of CH_3O produces a hydrogen atom and a formaldehyde molecule, providing the following important chain processes at high temperatures:

$$CH_3O + M \xrightarrow{k_1} H + CH_2O + M \quad (1)$$

$$H + CH_2O \rightarrow CHO + H_2 \quad (2)$$

$$CHO + M \rightarrow H + CO + M \quad (3)$$

These rapid chain reactions also prevent kineticists from directly and reliably determining the values of k_1, the rate constant for the unimolecular decomposition of the CH_3O radical.

All of the values of k_1 used in the literature for numerical modeling of combustion processes are derived either from indirect modeling involving complex chemistry or from theoretical calculations based on estimated thermochemical data.[2,3] To our knowledge, there have been no accurate kinetic data on reaction 1 in the literature that derive from direct rate measurements. Since neither the forward nor the reverse barrier of reaction 1 has been experimentally determined, theoretically predicted values using statistical unimolecular reaction rate theories (such as RRK or RRKM)[2,4] are not expected to be very reliable. The problem becomes worse if the reverse barrier is large, wherein tunneling effect may be significant.

In this study, we have experimentally extended our previous study of the thermal decomposition of CH_3ONO[5] beyond 550 K, above which the decomposition of CH_3O becomes measurable by either FTIR product analysis in static cell experiments or CW CO laser resonance absorption using a shock tube.[6] Kinetically modeled values of k_1 have also been theoretically interpreted by using the RRKM theory based on the results of our detailed ab initio calculations for reaction 1.[7] These results are briefly reported herein.

Experimental Section

Two different methods were employed to estimate CH_3O decomposition rates using methyl nitrite as the radical source. In the experiments carried out with a static cell (V = 277.3 cm^3), various reaction products (CH_2O, CH_3OH, CO, NO, N_2O) were quantitatively analyzed by FTIR spectroscopy. A detailed discussion of sampling and the reaction system can be found in ref 5. Typically, 2–4% of CH_3ONO/He mixtures were pyrolized at temperatures between 550 and 700 K within a short time interval and the measured product yields computer-modeled on the basis

† Adjunct Professor of Chemistry, The Catholic University of America. Present address: Department of Chemistry, Emory University, Atlanta, GA 30322.

(1) Glassman, I. *Combustion*; Academic Press: New York, 1987.
(2) Tsang, W.; Hampson, R. F. *J. Phys. Chem. Ref. Data* **1986**, *15*, 1087.
(3) Warnatz, J. In *Combustion Chemistry*; Gardiner, W. C. Jr., Ed.; Springer-Verlag: New York, 1984, p 187.
(4) Greenhill, P. G.; O'Grady, B. V.; Gilbert, R. G. *Aust. J. Chem.* **1986**, *39*, 1929.
(5) He, Y.; Sanders, W. A.; Lin, M. C. *J. Phys. Chem.* **1988**, *92*, 5474.
(6) Choudhury, T. K.; He, Y.; Sanders, W. A.; Lin, M. C., manuscript in preparation.
(7) Page, M., to be published.

0022-3654/89/2093-4404$01.50/0

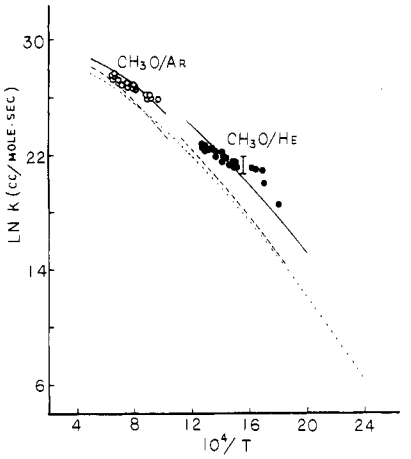

Figure 1. Comparison of theoretical and experimental values of the second-order rate constant for the methoxy radical decomposition reaction. Points are experimental data. Solid and long dash curves are RRKM results, with and without tunneling corrections, respectively. The dotted curve is the recommended value of Tsang and Hampson.[2] The shock tube data (1056–1666 K) is for 0.73 and 0.50% methyl nitrite in argon at pressures between 0.6 and 0.9 atm. The static cell data (550–700 K) is for 2.25 and 2.95% methyl nitrite in helium at a constant total pressure of 0.934 atm.

of the mechanism previously established to account for these product formation, particularly CO, CH_2O, and CH_3OH for the present purpose.

In our high-temperature experiments (T = 1060–1620 K), a shock tube, equipped with CW CO lasers for NO, CO, and H_2O diagnostics, was employed to measure these product yields. Typically, 0.1–0.7% CH_3ONO/Ar mixtures were pyrolized with incident shocks. The yield of H_2O was found to be negligible and that of NO remained constant and is of no kinetic value in this temperature region. Only CO yields changed rapidly with reaction time and were found to be strongly affected by the magnitude of k_1, according to the results of our kinetic modeling using a slightly more detailed mechanism to include high-temperature reaction processes such as HNO + M → H + NO + M, etc.[6,8] The kinetically modeled values of k_1, plotted in Arrhenius form, are presented in Figure 1. Because of space limitation, the measured and modeled product yields, as well as the reaction schemes are not listed in the present communication. Further description of the experiments is available as supplementary material (see paragraph at the end of the article regarding supplementary material).

Methyl nitrite was prepared by the dropwise addition of 30% H_2SO_4 to a saturated solution of $NaNO_2$ in methanol.[5] Gas product generated from the reaction was purified by trap-to-trap distillation using different slush baths. After purification with multiple distillations, the product was analyzed with FTIR. No detectable CH_3OH was noted in the purified sample.

Theoretical Section

The qualitative electronic structure changes taking place during methoxy decomposition are predominantly confined to three electrons and three molecular orbitals (MO's). The equilibrium and transition-state structures as well as the harmonic vibrational frequencies have thus been determined by using a three-electron, three-active orbital complete active space (CASSCF) wave function.[9] This is a multiconfiguration self-consistent field (MC-SCF) wave function formed by including all possible doublet configurations distributing the three active electrons among the three active orbitals. There are eight such configurations. At methoxy, the active MO's correspond to a C–H bonding and antibonding pair and a radical orbital localized on the oxygen atom. At the product formaldehyde, these orbitals correspond to the bonding and antibonding orbitals for the incipient π-type bond and the singly occupied orbital on the hydrogen atom.

TABLE I: MCSCF Structural Parameters[a]

	methoxy radical[b]		transition state		formaldehyde	
	DZP	TZP	DZP	TZP	DZP	TZP
C–H′	1.112	1.111	1.718	1.710	∞	∞
C–H	1.088	1.086	1.089	1.087	1.092	1.090
C–O	1.385	1.383	1.237	1.232	1.208	1.202
H′CO	106.2	106.1	102.5	102.5		
HCO	111.7	111.7	120.5	120.5	121.5	121.5
OCH′H	117.6	117.6	98.4	98.5	90.0	90.0

[a] Bond lengths are in angstroms; angles are in degrees. [b] $^2A'$ state.

TABLE II: MCSCF/DZP Harmonic Vibrational Frequencies[a]

sym	assignment	CH_3O[b]	H – CH_2O	H + CH_2O
a′	CHH s-stretch	3205	3183	3163
	CH′ stretch	2965	1396i	
	CHH bend	1636	1701	1636
	OCH_2 bend	1518	1201	1168
	CO stretch	1202	1558	1860
	OCH′ bend	1085	577	
a″	CHH a-stretch	3259	3278	3252
	CHHH′ deform	1519	745	
	CHHH′ rock	810	1328	1349
	zero-point energies[c]	24.6	19.4	17.8

[a] In cm^{-1}. [b] $^2A'$ state. [c] In kcal/mol.

The overall energetics are determined from single point calculations using configuration interaction CI wave functions involving all single and double excitations from all eight reference configurations. The multireference (MR)CI wave functions employed in this study are all obtained within the frozen core approximation. That is, the orbitals which correlate with the 1s core orbitals of carbon and oxygen along with the associated virtual orbitals are excluded in the configuration selection and are thus forced to be doubly occupied and unoccupied, respectively.

Two basis sets are used in this study. The first, denoted DZP, is the standard Dunning 4s/2p contraction[10] of the 9s/5p primitive set of Huzinaga[11] on carbon and oxygen with single d-polarization functions with exponents 0.75 on carbon and 0.85 on oxygen and the corresponding unscaled 4s/2s contraction on hydrogen with a single p-function of exponent 0.75. The second basis set, denoted TZP, is the 5s/3p contraction[10] of the same Gaussian primitive sets mentioned above augmented with the same polarization functions. There are 47 contracted basis functions in the DZP basis set and 58 contracted functions in the TZP. The MRCI calculations described above include 193 000 configurations in the DZP basis set and 329 000 configurations in the TZP basis set. The electronic structure calculations were all carried out on the Cray XMP-24 at the Naval Research Laboratory using the MESA[12] system of programs.

Fully optimized MCSCF geometrical parameters for the $^2A'$ Jahn–Teller distorted state of the methoxy radical, the dissociation transition state, and the product formaldehyde are given in Table I. The MCSCF structure for the methoxy radical is very similar to the UHF/6-31G* and /6-31G** structures reported by Saebo, Radom, and Schaefer[13] (hereafter SRS) in their extensive study of the Jahn–Teller splitting in methoxy and the rearrangement of methoxy to hydroxymethyl radical. An exception is the expected[14] lengthening of the in-plane CH bond (0.022 Å) which

(8) Choudhury, T. K.; Lin, M. C. "Pyrolysis of Mixtures of Methyl Nitrite and 1,3,5 Trioxane in Shock Waves: Kinetic Modeling of the H + CH_2O Reaction Rate". *Combust. Sci. Technol.*, submitted for publication.

(9) Roos, B. O.; Taylor, R. R.; Siegbahn, P. E. M. *Chem. Phys.* **1980**, *48*, 152.

(10) Dunning, T. H., Jr. *J. Chem. Phys.* **1970**, *53*, 2823. Dunning, T. H.; Hay, P. J. In *Modern Theoretical Chemistry*; *Vol. 3. Methods of Electronic Structure Theory*; Schaefer H. F. III, Ed.; Plenum Press: New York, 1977.

(11) Huzinaga, S. *J. Chem. Phys.* **1965**, *42*, 1293.

(12) MESA (Molecular Electronic Structure Applications); Saxe, P., Lengsfield, B. H., Martin, R., and Page, M.

(13) Saebo, S.; Radom, L.; Schaefer, H. F. *J. Chem. Phys.* **1983**, *78*, 845.

(14) Defrees, D. J.; Binkley, J. S.; Mclean, A. D. *J. Chem. Phys.* **1980**, *80*, 8.

TABLE III: Calculated Barriers[a] to Unimolecular Decomposition of the Methoxy Radical and the Reverse H Atom Addition to Formaldehyde

	forward barrier		reverse barrier	
	MCSCF	MRCI	MCSCF	MRCI
DZP	27.5	26.4	12.2	8.0
TZP	26.6	25.6	12.4	8.0

[a] In kcal/mol; barriers include zero point energy correction.

is correlated at the MCSCF level.

Harmonic vibrational frequencies and resulting zero point vibrational energies computed at the MCSCF/DZP level are presented in Table II. The assignments of the frequencies represent the most important contribution to the vibrational modes for the methoxy radical. Frequencies for the dissociation transition state and for formaldehyde are listed according to how they appear to correlate (i.e., in a vibrationally adiabatic picture) with the modes of methoxy. With the localized correlation of the CASSCF wave function, most of the geometrical degrees of freedom are treated at essentially a Hartree–Fock-like level. Consequently, the frequencies are similar to the UHF/6-31G* frequencies reported by SRS.[13] Two exceptions are the in-plane CH stretch, which is correlated in the MCSCF, and the CH_3 rock which is found to be considerably lower at the MCSCF level (810 cm^{-1} at MCSCF/DZP vs 1283 cm^{-1} at UHF/6-31G*[13]).

The energetics for the forward and reverse barrier of reaction 1 computed at the MCSCF//MCSCF and MRCI//MCSCF level for the two basis sets are given in Table III. Zero point energy corrections are computed from the (unscaled) harmonic frequencies in Table II. Our best computed values for the forward and reverse barriers of reaction 1, computed at the MRCI/TZP//MCSCF/TZP level of theory, are 25.6 and 8.0 kcal/mol, respectively. Both the forward and reverse barrier are found to be considerably lower than the MP3/6-31G** values of 34.4 and 12.4 kcal/mol reported by SRS, in accordance with their prediction.[13] The calculated endothermicity of reaction 1 ($\Delta H°$ = 17.6 kcal/mol) is 1.9 kcal/mol lower than the endothermicity calculated with the thermochemical data recommended in ref 2.

From the transition-state structure, vibrational frequencies, and energetics reported in Tables I–III, the dissociation transition state cannot be considered "loose" as can the transition states of many other dissociation reactions. The CH bond length at the transition state is only about 1.6 times the equilibrium value in methoxy. The frequencies of the "transitional modes", which by definition are zero at the product, attain about half of their full value at the transition state. Finally, there is an appreciable reverse energy barrier of 8.0 kcal/mol.

The potential energy surface information described above was used to calculate the rate of unimolecular decomposition of the methoxy radical by a standard RRKM procedure[15] modified to include quantum mechanical tunneling.[16,17] MCSCF/TZP structural parameters were used for the reactant and transition state. Harmonic vibrational frequencies used were those calculated at the MCSCF/DZP level of theory and the overall energetics were obtained from single-point MRCI/TZP calculations at the MCSCF/TZP structures.

In light of the appreciable reverse barrier found for reaction 1, and the fact that motion along the reaction coordinate is predominantly that of a hydrogen atom, it was felt that quantum mechanical tunneling might play a role in the decomposition rate. As discussed by Garrett and Truhlar[16] and Miller,[17] tunneling does not enter into the RRKM rate expression as a simple multiplicative factor as it does in standard (canonical) transition-state theory for bimolecular reactions. Rather the tunneling correction appears in a more convoluted manner, being incorporated into the microcanonical (energy dependent) rate constant.

The standard RRKM expression for the microcanonical rate constant is

$$k(E) = \frac{N(E)}{2\pi\hbar\rho(E)} = \frac{\sum_n h(E-\epsilon_n^\dagger)}{2\pi\hbar\rho(E)} \quad (4)$$

where $\rho(E)$ is the density of states of the reactant and the numerator is the sum of states in the degrees of freedom orthogonal to the reaction coordinate at the transition state. For a given state, $E - \epsilon_n^\dagger$ is the energy "left over" to traverse the barrier and $h(E-\epsilon_n)$ is a step function. Conceptually then, one is counting all possible states and assigning a weight of either unity or zero depending on whether $E-\epsilon_n^\dagger$ is positive or negative, respectively. Garrett and Truhlar's[16] and Miller's[17] modification to include tunneling involves replacing the step function $h(E-\epsilon_n)$ with the quantum mechanical probability of transmission through the barrier at energy $E - \epsilon_n^\dagger$,

$$k_{QM}(E) = \frac{\sum_n P(E-\epsilon_n^\dagger)}{2\pi\hbar\rho(E)} \quad (5)$$

Note that nonclassical reflection at energies above the barrier is included as well as tunneling at energies below the barrier.

The function $P(E-\epsilon_n^\dagger)$ is taken in the present calculations to be the probability of transmission through an Eckart barrier.[18] The three parameters defining the Eckart function are taken from the ab initio potential energy surface calculations. The barrier height and endothermicity are the zero point corrected MRCI/TZP values of 25.6 and 17.6 kcal/mol. The one remaining parameter is the curvature of the potential at the maximum. This was chosen to be the curvature of the MCSCF/DZP vibrationally adiabatic potential energy curve. That is, the shape of the bare barrier was modified to reflect the variation in zero point vibrational energy along the reaction coordinate in the vicinity of the saddle point. In determining this variation, a parabolic step was taken off the saddle point in either direction and two additional steps in each direction along the minimum energy path were taken using the LQA method.[19] Away from the saddle point, the reaction path direction as well as rotations and translations were projected out of the force constant matrices and harmonic normal mode analyses were performed. The transverse frequencies and resulting zero point vibrational energies were thus determined at seven points along the minimum energy path between arc lengths of $s = \pm 0.15$ $amu^{1/2}$ bohr. The maximum in the vibrationally adiabatic potential was found to be shifted to $s = -0.05$ $amu^{1/2}$ bohr, i.e., toward methoxy. The curvature of the vibrationally adiabatic potential at the maximum (0.093 hartree/$bohr^2$) was found to be greater than the curvature of the bare barrier (0.073 hartree/$bohr^2$).

Given these Eckart parameters, the probability of passage through the barrier at a given energy is given by a simple analytic expression.[20] Direct state counts, using the quantum mechanical transmission probability, were performed for energies ranging from 8.0 kcal/mol below the barrier to 30.0 kcal/mol above the barrier. For energies more than 30 kcal/mol above the barrier, the states were counted by using the Whitten–Rabinovich approximation.[15] The microcanonical rate constant as a function of energy was then computed by using eq 5. Note that all of the parameters necessary for this calculation were determined from ab initio calculations and nothing was scaled or otherwise estimated.

Results and Discussion

RRKM calculations were performed with a computer program previously used for the thermal decomposition of ethyl and methoxymethyl radicals,[21] with modifications to take into account the tunneling effect and the assumption of weak collisions between CH_3O and dilutent using Troe's approximation.[22] The average

(15) Robinson, P. J.; Holbrook, K. A. *Unimolecular Reactions*; Wiley: London, 1972. Forst, W. *Theory of Unimolecular Reactions*; Academic Press: New York, 1973.
(16) Garrett, B. C.; Truhlar, D. G. *J. Phys. Chem.* **1979**, *79*, 1079.
(17) Miller, W. H. *J. Am. Chem. Soc.* **1979**, *101*, 6810.
(18) Eckart, C. *Phys. Rev.* **1930**, *35*, 1303. Johnston, H. S. *Gas Phase Reaction Rate Theory*; Ronald Press: New York, 1966.
(19) Page, M.; McIver, J. W., Jr. *J. Chem. Phys.* **1988**, *88*, 922.
(20) See for example: Garrett, B. C.; Truhlar, D. G. *J. Phys. Chem.* **1979**, *79*, 2921.
(21) Lin, M. C.; Laidler, K. J. *Trans. Faraday Soc.* **1979**, *64*, 79.

energy transferred per collision ($-\langle\Delta E\rangle$) was taken to be 0.57 and 1.4 kcal/mol for Ar[4] and He, respectively. Based on our own RRKM calculations, those of Greenhill et al.,[4] and those of Tsang et al.,[2] the CH_3O decomposition reaction is effectively in the second-order region under the conditions employed. The calculated rate constant therefore varies with the assumed collision efficiency of bath gases. The values for $-\langle\Delta E\rangle$ assumed are essentially within the range found for monatomic gases, 0.5–2.0 kcal/mol.[22]

The calculated values of the second-order rate constant, k_1, with and without tunneling correction are compared to the experimental ones in Figure 1. Also included in the figure is the calculated value by Tsang and Hampson[2] for N_2 based on the high-pressure, first-order rate constant estimated by Batt[23] who recomended an activation energy of 27.5 kcal/mol for the decomposition of CH_3O. Because of the closeness of the $\langle\Delta E\rangle$ value assumed for N_2, 1.3 kcal/mol, Tsang's value agrees reasonably closely with our calculated values for both Ar and He without tunneling correction (i.e., the long-dashed curves in Figure 1). The tunneling correction increases the value of k_1 by a factor of 18 at 500 K and a factor of 4.5 at 1000 K. The theoretical values with tunneling correction agree reasonably well with the modeled k_1 values above 700 K. Because of the low CO yields at lower temperatures ($\leq$700 K), the reliability of the data at these temperatures is not expected to be better than $\pm$100%, as denoted by the error bar shown in the figure. It is interesting to note that the calculated RRKM curve by Greenhill et at.[4] using E_0 = 24.0 kcal/mol and $-\langle\Delta E\rangle$ = 0.57 agrees closely with our solid curves which include tunneling corrections.

The rate of unimolecular reactions in the low-pressure (second-order) limit is controlled by the rate of collisional activation, which depends on the threshold energy for reaction. The *absolute* low-pressure limit, when tunneling is considered, is only reached at extremely low pressures. This is because any molecule which is collisionally activated to an energy that is above the product asymptote has a finite lifetime, even though it may be well below the classical threshold for reaction. To achieve the true low-pressure limit, the rate of collisional deactivation must be slow compared to the lifetime of all such states. However, since the microcanonical rate constant, $k(E)$, falls off very rapidly at energies more than a few kcal/mol below the classical threshold, an effective second-order region is reached long before this condition is met. The calculated falloff curves with and without tunneling corrections for the high- and low-temperature regions are shown in Figure 2. Figure 2a compares the pressure falloff curves for calculations using argon as a bath gas at T = 1300 K. Figure 2b is the analogous comparison at T = 600 K in helium. As expected, tunneling is generally more important at lower temperatures. At 710 Torr (log P = 2.85), the falloff curves without tunneling predict the reaction to be completely in the second-order region. When tunneling is considered, the reaction is seen to still be essentially in the second-order region, although as discussed earlier, the true low-pressure limit is not reached until the pressure is extremely low.

In the absence of tunneling, the low-pressure rate is insensitive to features of the potential energy surface in the vicinity of the activated complex, other than the barrier height itself. Tunneling lowers the effective threshold energy for reaction, allowing molecules to react which are collisionally activated to an energy which is *below* the classical barrier height. This lowering of the reaction threshold, and the resulting enhancement of this *effective* low-pressure reaction rate, depend critically on features of the potential energy surface in the vicinity of the activated complex.

The absolute magnitude of the calculated rate constant depends critically on the calculated value for the classical energy threshold for reaction. Uncertainties in the threshold energy come from several sources: basis set truncation, inaccuracies in stationary point structures and zero point energy differences, and incomplete description of correlation energy changes. Since the resulting uncertainty in the barrier height may be in the range of 2–3 kcal/mol, one cannot say that the agreement between theory and experiment depicted in Figure 1 *demands* the presence of a significant tunneling contribution to the rate. On the other hand, for a given activation energy, the rate enhancement due to tunneling depends on specific features of the potential energy surface, the influence of which can be assessed. We have neglected in these calculations the effect of reaction path curvature. Inclusion of this effect essentially lowers the effective mass for the barrier penetration problem and would increase the magnitude of the calculated tunneling contribution. The tunneling contribution to the rate is expected to be most sensitive to the width of the barrier near the maximum. For the Eckart potential, this is largly determined by the parameter representing the curvature of the potential energy barrier at the maximum. This curvature was computed at the MCSCF/DZP level for which the reverse barrier for reaction 1 is 12.2 kcal/mol. Since this is 4.2 kcal/mol higher than the MRCI/TZP barrier, the curvature may be overestimated. To test the effect of this parameter, the calculations were rerun

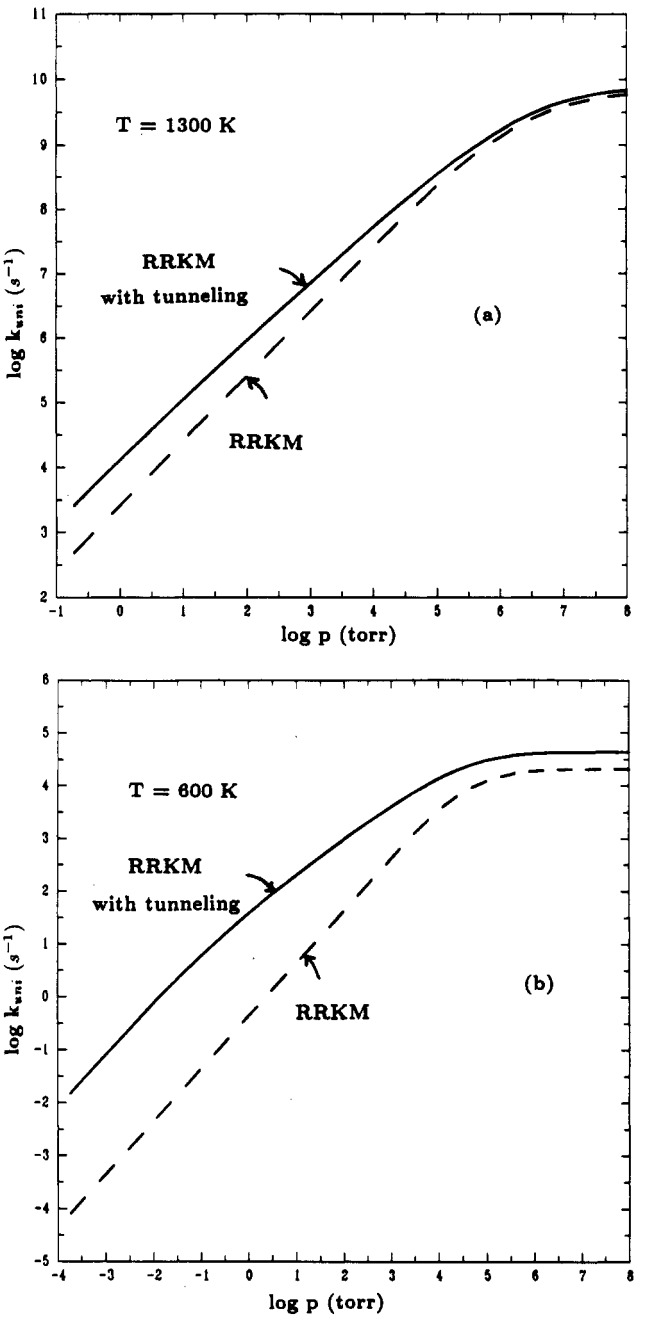

Figure 2. Calculated unimolecular pressure falloff curves for the reaction $CH_3O + M \rightarrow CH_2O + H + M$ at T = 1300 K in argon (a) and at 600 K in helium (b). The RRKM with tunneling curves are represented by solid lines and the RRKM without tunneling curves are represented by dashed lines.

(22) Troe, J. *J. Phys. Chem.* **1979**, *83*, 114.
(23) Batt, L. *Int. J. Chem. Kinet.* **1979**, *11*, 977.

with the curvature arbitrarily (and somewhat drastically) cut in half. The resulting tunneling curve moved only about one-third of the way (in a logarithmic sense as in Figure 1) toward the no-tunneling curve. We conclude from the present study that there is an appreciable contribution to the rate of methoxy radical decomposition due to quantum mechanical effects along the reaction coordinate.

For the convenience of high-temperature kinetic modeling, we have analyzed our experimental data by ignoring the minor difference in collision efficiency between Ar and He, using both linear and nonlinear least-squares methods. These analyses give rise to[6]

$$k_1 = (5.5 \pm 0.6) \times 10^{13} \exp(-6790 \pm 102/T)\ \mathrm{cm^3/(mol\cdot s)}$$

and

$$k_1 = 8.3 \times 10^{17} T^{-1.2} \exp(-7800/T)\ \mathrm{cm^3/(mol\cdot s)}$$

for the temperature range of 550-1620 K.

Acknowledgment. Y.H. and T.K.C. acknowledge the U.S. Department of Energy, Office of Basic Energy Sciences, Division of Chemical Sciences, for support of this work through contract DE-FG05-85-ER13373. M.P. and M.C.L. acknowledge support of the Office of Naval Research through the Naval Research Laboratory.

Supplementary Material Available: Table showing reaction scheme and rate coefficients used in kinetic modeling, Figures 3 and 4 showing effects of changes in rate of reaction on CO production (6 pages). Ordering information is given on any current masthead page.

Picosecond Transient Absorption Spectroscopy of Polysilanes

Y. Ohsako,[†] J. R. G. Thorne,[†] C. M. Phillips,[†] J. M. Zeigler,[‡] and R. M. Hochstrasser*,[†]

Department of Chemistry, University of Pennsylvania, Philadelphia, Pennsylvania 19104-6323, and Sandia National Laboratories, Albuquerque, New Mexico 87185 *(Received: October 13, 1988; In Final Form: February 23, 1989)*

Transient absorption spectra have been recorded in the range 350-750 nm in solution at room temperature for *poly(phenylmethylsilane)*. A transient absorption band at 450 nm resembles that of PhMeSi, and a band at 370 nm is another product. Both rise time and decay times of the transients were determined. Room temperature "hole burning" of the absorption spectrum is reported.

Introduction

The mechanism of bond cleavage of polysilanes is of current importance because of their applications as photoresists and photoinitiators. The details of the photochemical processes are poorly understood for the alkyl and aryl substituted materials both in solution and in the solid state. Evidence for intermediates involved has come from trapping studies,[1] cross-linked/scission product ratios,[2] mass spectroscopy,[3] and ESR studies.[4] There have been recent transient absorption studies on the lower molecular weight materials that might serve as models for the photochemical decay. Different workers have examined cyclo-$(SiMe_2)_6$[5,6] and $PhMeSi(SiMe_3)_2$[7a] and ascribed induced absorptions near 450 nm to the silylene biradicals Me_2Si and PhMeSi. A picosecond study on the properties of the phenyldisilane, $PhSiMe_2SiMe_3$, ascribes a 425-nm transient to a silene.[8] We are unaware of any transient absorption studies on the high polymers except for those induced by pulsed electron bombardment producing radical anions.[9]

The lowest energy optical excitation in poly(phenylmethylsilane) occurs at ~340 nm and is nearly resonant with emission at ~353 nm.[10,11a] We have recently begun a study of the optical properties of the polysilanes using the techniques of time-correlated single-photon counting to measure fluorescence lifetimes and fluorescence anisotropy decays,[12a,13] to establish the nature of the excited state. This excitation is estimated to be delocalized over several tens of silicon atoms.[12a,b] In addition in poly(phenylmethylsilane) broad long-wavelength emissions centered at about 430 nm are observed which have been variously attributed to triplet-state phosphorescence,[11a,14] to photoproduct impurity,[15] and to a charge-transfer state.[16] Because of the structured emission, indicative of a narrower bandwidth or localized excitation, this state has been assumed to be the precursor to photochemistry.[11a,14] Excited-state charge transfer from the silicon-silicon bond to the phenyl ring would not be inconsistent with the band structure calculations[17] and might assist charge separation in the excited

[†] University of Pennsylvania.
[‡] Sandia National Laboratories.

(1) (a) Trefonas, P.; West, R.; Miller, R. D. *J. Am. Chem. Soc.* **1985**, *107*, 2737. (b) Michl, J.; Downing, J. W.; Karatsu, T.; McKinley, A. J.; Poggi, G.; Wallraff, G. M.; Sooriyakumaran, R.; Miller, R. D. *Pure Appl. Chem.* **1988**, *60*, 959.
(2) Trefonas, P.; West, R.; Miller, R. D.; Hofer, D. *J. Polym. Sci., Polym. Lett. Ed.* **1983**, *21*, 823.
(3) (a) Zeigler, J. M.; Harrah, L. A.; Johnson, A. W. Advances in Resist Technology and Processing II; *Proc. of SPIE Int. Soc. Opt. Eng.* **1985**, *539*, 166. (b) Magnera, T. F.; Balaji, V.; Michl, J.; Miller, R. D. *Silicon Chemistry*; Corey, Corey, Gaspar, Eds.; Ellis Horwood: Chichester, 1988; Chapter 45.
(4) Michl, J.; Downing, J. W.; Karatsu, T.; Klingensmith, K. A.; Wallraff, G. M.; Miller, R. D. *Organometallics* **1988**, *7*, 2567.
(5) Drahnak, T. J..; Michl, J.; West, R. *J. Am. Chem. Soc.* **1979**, *101*, 5427.
(6) Shizuka, H.; Tanaka, H.; Tonokura, K.; Ohshita, J.; Ishikawa, M. *Chem. Phys. Lett.* **1988**, *143*, 225.
(7) (a) Gaspar, P. P.; Holten, D.; Konieczny, S. *Acc. Chem. Res.* **1987**, *20*, 329. (b) Gillette, G. R.; Noren, G. H.; West, R. *Organometallics* **1987**, *6*, 2617.
(8) Shizuka, H.; Okazaki, K.; Tanaka, M.; Ishikawa, M.; Sumitani, M.; Yoshihara, K. *Chem. Phys. Lett.* **1985**, *113*, 89.
(9) Ban, H.; Sukegawa, K.; Tagawa, S. *Macromolecules* **1988**, *21*, 45.
(10) Harrah, L. A.; Zeigler, J. M. *Macromolecules* **1987**, *20*, 601.
(11) (a) Harrah, L. A.; Zeigler, J. M. In Hoyle, C. E., Torkelson, J. M., Eds.; ACS Symposium Series 358; 1987; p 482. (b) Klingensmith, K. A.; Downing, J. W.; Miller, R. D.; Michl, J. *J. Am. Chem. Soc.* **1986**, *108*, 7438. (c) Johnson, G. E.; McGrane, K. *Polym. Prepr.* **1986**, *27*, 352.
(12) (a) Kim, Y. R.; Lee, M.; Thorne, J. R. G.; Hochstrasser, R. M.; Zeigler, J. M. *Chem. Phys. Lett.* **1988**, *145*, 75. (b) Michl, J.; Downing, J. W.; Karatsu, T.; Klingensmith, K. A.; Wallraff, G. M.; Miller, R. D. *Inorganic and Organometallic Polymers*; Zeldin, Wynne, Allcock, Eds.; ACS Symposium Series 360; American Chemical Society: Washington, DC; 1988; Chapter 5, p 61.
(13) Thorne, J. R. G.; Hochstrasser, R. M.; Zeigler, J. M. *J. Phys. Chem.* **1988**, *92*, 4275.
(14) Harrah, L. A.; Zeigler, J. M. *J. Polym. Sci. C: Polym. Lett.* **1987**, *25*, 205.
(15) Harrah, L. A.; Zeigler, J. M. *Polym. Prepr.* **1986**, *27*, 356.
(16) Kagawa, T.; Fujino, M.; Takeda, K.; Matsumoto, N. *Solid State Commun.* **1986**, *57*, 635.

0022-3654/89/2093-4408$01.50/0